Stress Concentration Analysis and Fabrication of Silicon (100) Based Ultra-Stretchable Structures with Parylene Coating

Mutee Ur Rehman,[a] Wedyan Babatain,[b] Sohail Faizan Shaikh,[b] David Conchouso,[b,c] Nadeem Qaiser,[b] Muhammad Mustafa Hussain,[b] and Jhonathan Prieto Rojas[a,*]

[a]*Electrical Engineering, King Fahd University of Petroleum and Minerals, Dhahran 31261, Saudi Arabia*
[b]*Computer, Electrical and Mathematical Sciences & Engineering Division, King Abdullah University of Science and Technology, Thuwal 23955, Saudi Arabia*
[c]*Escuela de Ingeniería, Universidad Anáhuac Puebla, Puebla 72810, México.*
* Corresponding author
E-mail addresses: muteeurehman@gmail.com (M. U. Rehman), wedyan.babatain@kaust.edu.sa (W. Babatain), sohailfaizan.shaikh@kaust.edu.sa (S. F. Shaikh), david.conchousogo@anahuac.mx (D. Conchouso), nadeem.qaiser@kaust.edu.sa (N.Qaiser), MuhammadMustafa.Hussain@kaust.edu.sa (M. M. Hussain), jprojas@kfupm.edu.sa (J. P. Rojas)

Abstract

Research in stretchable electronics is helping to revolutionize the current electronic industry, particularly in wearable and bio-integrated devices. Cost-effectiveness and easy manufacturing are key factors that contribute to shaping the fate of such technologies. In this work, we present a fabrication method for a novel ultra-stretchable, serpentine-arm spiral (SAS) that was built using a low-cost, standard bulk silicon (100) wafer. However, structural defects that often appear during patterning processes, can lead to stress concentration and structural failure at these sites upon stretching. Parylene coating of the structures is proposed to minimize this stress concentration and improve structure's robustness. Finite element analysis (FEA) was performed to demonstrate the concentration of stress at these defective sites with 2 sizes (0.1 μm and 1 μm) and at different locations along the arms. Results show that SAS structures reach up to ~80% stress reduction at the defective location compared to straight-arm spirals, while the parylene-coating helps to reduce it up to ~60% further. On the other hand, fabricated uncoated, SAS structures reached up to ~600% prescribed strain before fracture, while parylene-coating improves this maximum admissible strain in ~50%. Additionally, a cyclic tensile test

was then performed on the fabricated structures, uncoated and parylene-coated, for over 3000 cycles without fracture. The results observed on coated structures greatly improve the mechanical reliance of such brittle structures, which could be extended to other stretchable configurations.

Keywords: Spiral, Serpentine, Silicon, Parylene, Stretchable Electronics, Finite Element Analysis.

1. Introduction

Flexible and stretchable electronics are paving their way into the market at a very high pace due to their applications in bio-integrated systems [1], wearable technology [2], and soft-robotics [3], among others. However, interaction between electronics and soft, flexible and stretchable biological systems is a persistent challenge. Development of novel electronic devices, capable of adjusting to flexible systems while maintaining high electrical performance, are greatly desired [4].

Generally, there are two main approaches employed in the design of flexible and stretchable electronics; (i) Using novel materials (i.e. inherently flexible/stretchable) with limited electrical properties that need to be improved, or (ii) Designing innovative flexible/stretchable structures into conventional materials (polymers, conductors and semiconductors) that may have already great electrical performance but a brittle mechanical behavior [4–11]. For the first approach, conductive nanocomposites and nanomaterials have been tested to improve applications in areas such as optoelectronics, and energy harvesting among others [12,13]. These softer polymeric materials appear to be the natural choice for flexible and stretchable electronics [10,14]. However, they still lack the electrical performance needed by many applications that demand high data processing [4,15–20].

Silicon, on the other hand, is the predominant choice in the standard electronics industry because of its abundance, well-established processing techniques and its outstanding performance. However, it is a

brittle material that breaks easily under shearing stress and thus has poor mechanical performance for flexible and stretchable applications.

Even though there are many challenges in processing silicon as a flexible material, it currently leads the field of inorganic-based, flexible and stretchable electronics [8,9], as it becomes surprisingly flexible when thinned down to micro- or nanoscale (silicon ribbons of 100 nm thickness experience peak strains of barely 0.0005% at 1 cm of bending radii) [4,21,22]. In the same way, adequate structural modifications in these thinned materials can render them stretchable [23–26]. For example, nano-membranes that were shaped as a serpentine structure showed improved stretchability because of its advantageous spring-like geometry [27].

Since both conventional materials and flexible polymers present advantages and challenges in the development of flexible and stretchable electronics, a convenient approach is to combine the advantages of both worlds and expanding the silicon's mechanical abilities by the support of softer polymeric materials.

One way of combining both material sets is by transferring silicon nano-membranes onto polymeric substrates. This strategy reduces the mechanical stress at the structure, while maintaining the excellent electrical properties of silicon [8,9]. Similarly, placing the silicon structure at the neutral mechanical plane, by sandwiching it in-between soft materials, can improve the mechanical performance by reducing the stress on the less elastic silicon [28]. In fact, such heterostructures that combine soft and rigid materials have been a key factor in the development of flexible and stretchable electronics [2]. This line of thought guided us, in this paper, to explore the idea of creating compound structures that are fabricated in silicon and coated with a polymer, as will be discussed later on.

Another structural modification that resulted into a mechanically efficient stretchable system is to distribute the rigid elements into a mesh-like structure. This configuration can be done by island-

interconnecting arrangements, where rigid islands host the electronics and the mechanically adaptable interconnects provide the stretchability of the structure [29–34]. This novel arrangement minimizes the stress experienced at the more vital electronic components during bending and stretching [35].

Different system's components, such as power management, sensor modules, communication, etc., can be distributed and reorganized throughout the array of islands depending on the application [6,24].

Unlike islands, the interconnects have a geometry that is designed for stretching such as serpentine-based interconnects and others [36]. These serpentine interconnects can also be used to place electrical tracks to communicate between the two or more islands. Additionally, in the work demonstrated by Kim *et al.*, polymeric encapsulation was essential to ensure the system's mechanical robustness, by placing the fragile electronic circuits at the neutral mechanical plane, and allowing a large deformation to be achieved by the serpentine interconnects [37].

In optimizing the performance of these interconnects, some works have included fractal-inspired features to the interconnects, which have demonstrated an enhanced mechanical behavior in the structures [38–40].

In addition to serpentine structures, spiral-based interconnects have also been studied. These structures display the highest stretchability among the studied structures, and thanks to its compact in-plane area, become very convenient island-interconnection schemes [41]. In fact, a topology of silicon-based, circular islands physically interconnected through silicon-spiral-springs in a 2D network was previously demonstrated, showing a 51-times area increase upon stretch [42]. More recently, this platform was used to build a photodiodes' array and form a fully stretchable spherical 360° imaging system, hence demonstrating its great potential in unique applications [24]. Similarly, island-interconnect-based platforms have been used to build a sensing mechanism to detect the movement of islands upon external strain. This sensing mechanism can used in applications such as soft robotic arms, among others [43].

Moreover, the same designs have been studied in various array configurations and stretchable networks due to their improved mechanical robustness [44]. Finally, it is important to clarify that such demonstrations have been designed to work without the need for underlying, soft substrates, but as stand-alone stretchable structures. This type of interconnected islands through silicon spiral springs will be the center of this study.

On a separate matter, it should be noted that structural defects might occur during the fabrication of micro/nano devices, depending on the resolution of the photolithographic system and other processes involved during patterning. For example, line edge roughness (LER) or presence of particles, can lead to imperfections in the range of tens of nanometers to tens of micrometers along the spiral's arms [45,46]. Presence of defects that may arise during fabrication has been identified for a long time to affect the performance of a great variety of applications ranging from integrated circuits to micromachined silicon membranes [47,48]. In relation to mechanical performance, it has been already demonstrated that a thermal-oxidation-based surface treatment can assist in reducing defects along the vertical spring arms in a spiral-based island-array, producing smoother wall surfaces and achieving higher strain compared to untreated structures [42]. Nevertheless, thermal oxidation is a restrictive process due to its very high thermal budget, so we propose an alternative and more approachable polymer-coating scheme that can help in reducing the stress concentration and thus achieve higher elongation ratios.

In this work, we first present a cost-effective way to fabricate novel serpentine-arm spiral (SAS) silicon structures compared to previous fabrication approaches of similar structures. Horseshoe structures are also added both at the beginning and end of the arms to reduced structure's stress concentration as it has been previously demonstrated [25,49]. Moreover, and as mentioned above, inorganic structures can be transferred to or encapsulated in polymeric substrates for improved mechanical performance. Therefore,

we have chosen a similar approach, coating the silicon structures using a highly conformal parylene C layer. Conformality ensures excellent coverage of the silicon structures, filling any structural defects that may appear during fabrication. Finite element analysis (FEA) is used to study the effect of such defects at the interconnects and whether the integration of polymer coating can assist in the reduction of any stress concentration. Finally, tensile and cyclic tests are performed on the fabricated structures to observe their mechanical robustness.

We believe this work will provide useful insights into the mechanical response, under extreme strain conditions, of stretchable interconnects and the effects of defects along them, as well as the use of polymer coating as a practical approach to further extend the achievable stretchability of the structures.

2. Materials and Methods

2.1 Fabrication of silicon (100) based SAS structures

As mentioned above, island-interconnect designs based on inorganic materials such as silicon have attracted a lot of attention in the field of stretchable electronics. These structural designs not only provide stretchability but also provide freedom to the designer to spatially distribute electronic components for efficient system design. The rigid part of the structures, in our case the area in middle of the spirals, can be used to host electronic components where they will experience no stress, while the arms of the spiral can stretch. Therefore, here we present a fabrication approach, based on a bulk, low-cost silicon (100) wafer, of such spiral structures with optimized serpentine-arms, which were proposed and described in detail in a previous work [25]. The fabrication method consists of peeling-off a thin layer containing the flexible structures from the surface of a mono-crystalline, bulk silicon (100) wafer through various sequential etching steps.

This technique allows for re-using the remaining of the wafer to fabricate more structures, after a chemical mechanical polishing (CMP) process. As previously demonstrated, a single wafer can be reused to produce at least 5 thin silicon layers, making it a cost-effective fabrication method compared to previous fabrication approaches of similar structures [50,51]. In fact, the CMP step that is already involved in the bulk silicon wafer production, has been estimated to represent only a ~20% of the total substrate production cost [52]. Therefore, the recycling of a bulk substrate that only involves one CMP step, should represent a significant saving compared to the purchase of a new substrate. Additionally, it is to be noted that current polishing processes can achieve less than 0.3 nm root-mean-squared roughness, which is already sufficient for other sub-sequent processing involved in the manufacture of electronic devices [53]. Even smoother surfaces can also be achieved through a subsequent epitaxial silicon growth, reducing roughness and defects, which might be required for the fabrication of advanced integrated circuits at ultra-large-scale integration (ULSI) [54][55].

Our approach improves on previously demonstrated techniques that require the use of DRIE, a release process and a complete wafer to obtain the thinned silicon sheet with the stretchable structures. These previously developed approaches require either a silicon-on-Insulator (SOI) or silicon (111) substrates (typically five to two times more expensive than standard bulk silicon wafers), or consuming a whole bulk wafer for a single thinned sheet [21,24,56]. Additionally, aluminum was used as a hard mask to pattern the flexible and stretchable structures, instead of the more expensive Ti/Au mask that was used in a previous work [21]. Another benefit of our fabrication method is the controlled release of the structures from the wafer. Here we used a XeF_2 dry etching tool that can be easily timed, optimized and does not represent a significant cost increase to the total fabrication process, as it has been discussed in an earlier work [50]. Additionally, this dry scheme avoids the use of wet etchants that require post-

cleaning, complicate handling, can lead to stiction issues and might affect any device already fabricated on the structures.

Fig. 1 shows the detailed fabrication process. This procedure starts with a 4-inch mono crystalline silicon (100) wafer. The chosen (100) orientation is not only the cheapest and most wide-spread used silicon substrate, but also displays the highest electron transport mobility and less defect density compared to other orientations used in flexible electronics [57]. The doping type and concentration of the substrate should be chosen according to the application and will not affect the procedure steps describe here. The substrate is then protected with a 500 nm thick silicon dioxide (SiO_2) layer, which was grown using a dry-wet-dry oxidation technique in a tube furnace (1100°C, dry: 15 min., 3000 sccm O_2, wet: 36 min., 200 sccm O_2, dry: 15 min., 3000 sccm O_2, annealing: 20 min., 5000 sccm N_2). Next, we deposited a 200 nm Aluminum (Al) film on top of the SiO_2 by sputtering (400 W_{RF}, 600 seconds, 5 mTorr, Pre-sputter: 100 seconds, 25 sccm Ar), as shown in Fig. 1(a).

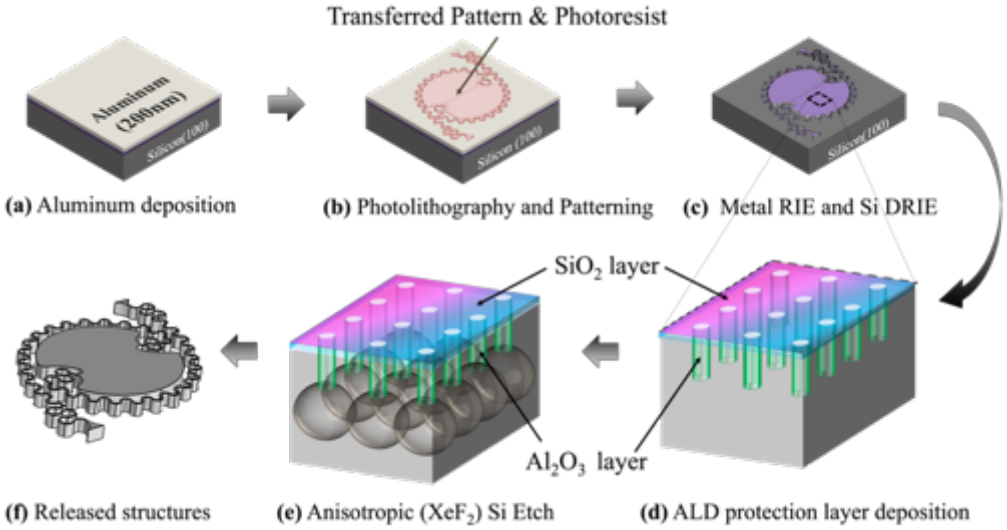

Fig. 1 Fabrication process flow of SAS structure detailing (a) sputtering of Al, (b) photolithographic pattering of the structure, (c) the Al and the SiO_2 RIE etching process, as well as the DRIE Si etch of the patterned structure, (d) Al_2O_3 deposition on sidewalls, (e) XeF_2 etch and (f) released silicon structure.

This metal was deposited to act as a hard mask to protect the silicon during the subsequent deep reactive ion etching (DRIE) process. The aluminum layer is patterned using a 4 μm ECI3027 photoresist and standard photolithography. (Fig. 1(b)). Next, reactive ion etching (RIE) was then used to selectively pattern the top Al, through a chlorine (Cl_2) -based etching (e.g.,100 W_{RF}, 40 mTorr, 10 sccm Cl_2, 40 sccm BCl_3 and 5 sccm Ar). Then the oxide layer was also selectively etched using fluorine based RIE (100 W_{RF}, 30 mTorr, 40 sccm C_4F_8, 5 sccm O_2). For DRIE, (Fig. 1(c)) gases containing fluorine were used to etch the silicon anisotropically creating vertical channels into the wafer (~50 μm, 200 cycles, 5 sccm C_4F_8, 100 sccm SF_6, 30 mTorr, 30 W_{RF}). For a successful DRIE, holes were used all over the design to provide a path for the gases to diffuse into the structure and etch the material isotropically, deep beneath the surface. Therefore, it is important that these holes are cleared from any metal or oxides at their bottoms. A ~90 nm thick Al_2O_3 was deposited using atomic layer deposition (ALD) to avoid any silicon loss at the lateral walls (TMA for 15 ms, H_2O_{vapor} for 15 ms, 900 cycles at 250°C) and then a highly directional RIE was used to clear-out the Al_2O_3 at the bottom surface of each hole (40 nm/min, 4 mTorr, 20 sccm CHF_3, 5 sccm Ar) (Fig. 1(d)). Finally, the structures were released using XeF_2 isotropic etching (85 cycles, 30 sec/cycle, 4 mTorr) (Fig. 1(e)). This isotropic etching releases the final structure from the substrate as shown in Fig. 1(f). Fig. 2(a) shows scanning electron microscopy (SEM) images after the DRIE process of the SAS structure (the zoom-in view shows the etching holes throughout the structure).

2.2 Structural defects and polymer coating

Since the structures are released from a standard silicon wafer as thin skins with narrow interconnects, any common fabrication defects can impact greatly the performance and reliability of the flexible and stretchable structures. Fig. 2(b) shows a representative, LER-based defect of ~0.1 μm in size, found

along one of the arms of a spiral. These defects may significantly affect the mechanical behavior of stretchable devices and therefore, their study will be an important component of this work.

On the other hand, and as mentioned earlier, locating the rigid silicon structure in the mechanical neutral plane of the system reduces the experienced mechanical stress. This could be achieved by coating the silicon structure with a soft-polymer material [58,59]. In our case, the purpose of the polymer coating was also to fill any lithographic defect with a material capable of withstanding large structural deformations. Parylene C was chosen as the coating material mainly due to its vapor-based deposition method that allows a truly conformal coating, which is ideal for this type of complex geometries that involve micrometer features. Moreover, parylene is also recognized by its biocompatibility, chemical inertness and low intrinsic stress, making it an excellent protective encapsulating barrier and a widely used polymer in flexible and stretchable electronics [60,61]. Other well-known polymers, such as SU8, polyimide, PMMA and PDMS, lack the advantageous conformality of parylene and cannot be deposited as desired. In fact, parylene's excellent conformality has been demonstrated to produce uniform, pinhole-free coatings down to even nanometric range in thickness, and being able to fill deep gaps and undercuts features beyond 500 nm in depth [62–66]. Such uniformity is of particular interest to ensure the conformal coverage of any small defect along the silicon structures. Similarly, other materials, such as oxides and metals, either do not provide an appropriate coating procedure (involving restrictive temperatures or chemistries) or are intrinsically too rigid and therefore not suitable for this work. Parylene coating was carried out at 690 C° using Lab coater2® (Model PDS 2010). 10 g of Parylene C was used for a target of 2 μm in thickness. SEM images in Fig. 2(c) show the parylene-coated SAS compound structure with and actual polymer thickness of ~3 μm. This thickness was chosen according with the 15μm-radius serpentines and their spacing.

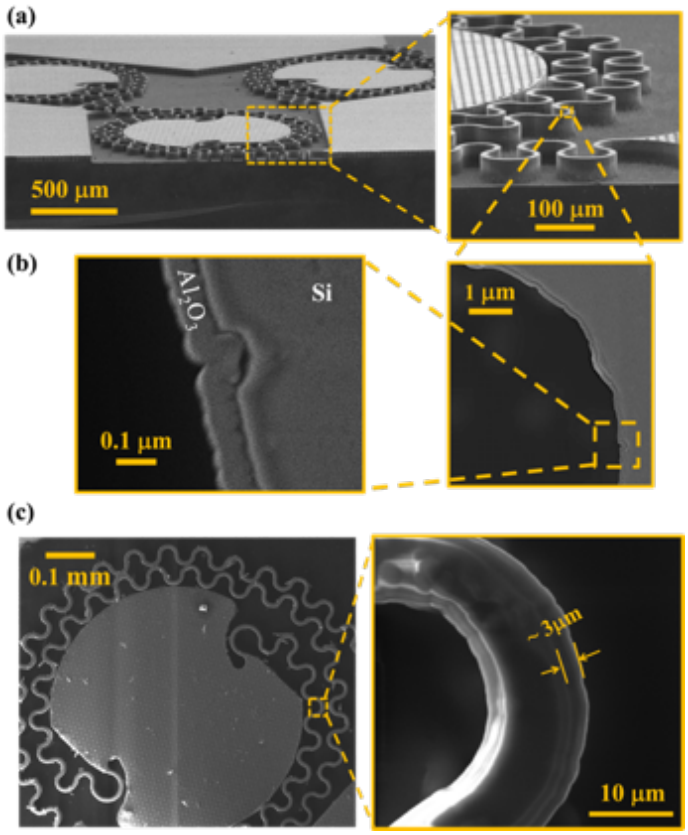

Fig. 2 (a) SEM images of SAS structure after DRIE including zoom-in view. (b) SEM image of a representative defect of ~0.1 µm in size, found along one of the arms of a spiral (the conformal layer along the geometry is the Al_2O_3 sidewall protection layer deposited in an earlier fabrication step). (c) SEM image of parylene-coated, SAS structure, including zoom-in of the arm showing the parylene thickness.

3. Spiral's Stretchability Model

It is worth mentioning that the maximum stretchability of a spiral structure with two arms, although dependent on several parameters, like radius, width of the arms and their spacing, it mainly depends on the total number of turns of both arms. Also, for simplicity and practical purposes, we will consider a simplified straight-arm spiral model. Fig. 3(a) shows the used spiral model structure, where *r* represents the radius of the inner circle, *S* represents the spacing between the arms, *w* represents the width of the arms of the spirals and *L* is the length of the extended ending of each arm.

In order to derive a simple model for the maximum applied strain of the structure shown in Fig. 3(a), we first notice that the initial length L_i of the structure without deformation is

$$L_i = 2L \tag{1}$$

Similarly, final length L_{f_max} when fully stretched at maximum displacement is

$$L_{f\_max} = 2\pi N\big(r + N(w+s)\big) + 2r + 2L \tag{2}$$

Where N represents the total number of turns of both arms (N = 2 in Fig 3(a)). Then, the maximum applied strain, ε_{max}, for N-turns spiral would be given from

$$\varepsilon_{max} = \frac{2\pi N\big(r+N(s+w)\big)+2r}{2L} \tag{3}$$

Finally, in our design we have selected the spacing between arms to be four times the width of the arms, so that there is enough space in the case we want to fit the serpentine-arms. Making $s = 4w$, the final equation becomes

$$\varepsilon_{max} = \frac{2\pi N(r+5Nw)+2r}{2L} \tag{4}$$

It should be noted that if w is much smaller than r, then N becomes the predominant factor in the equation. This means that by simply increasing or decreasing the number of turns in the spiral, the stretchability of the overall system can be controlled according to the nature of the application. In this demonstration, w = 5 μm, r = 250 μm, L = 323 μm, for which ε_{max} = 344.8% if N = 1, and ε_{max} = 661% if N = 2. Further design considerations and mechanical modeling can be found in previous works [21,25].

4. Results and Discussion

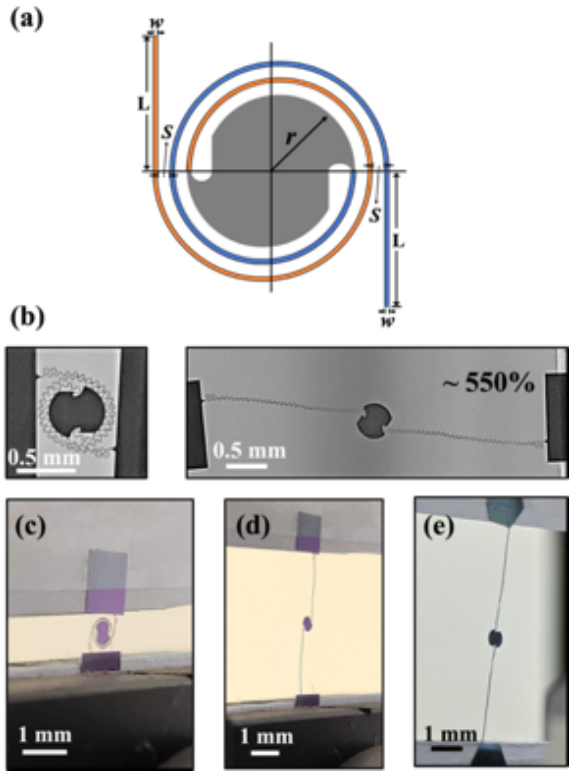

Fig. 3 (a) Schematic diagram of straight-arm spiral. (b) Optical-microscope photographs of a un-stretched and stretched SAS structure up to ~550% elongation, showing details of the serpentine-arms. (c) Un-stretched and (d) stretched SAS structure during tensile test, before fracture. (e) Fully stretched parylene-coated SAS compound structure. (Spiral arm's width is 5 μm and $N = 2$ for all cases).

In order to understand the mechanical resilience of the SAS design, the fabricated structures (with w = 5 μm, r = 250 μm, and $N = 2$) were subjected to a simple tensile test to check their maximum extension before fracture. Fig. 3(b) shows a SAS sample structure under a microscope, stretched to ~550%, in which the serpentines along the arms can be appreciated in detail. Next, a universal testing machine (Instron 3343) was used to test 3 separate samples. The structures were first carefully attached to a handling paper, then transferred into the tool, where they can be stretched up to their fracture. It should be noted that handling of the uncoated structures was challenging due to their brittle nature, however, their handling considerably improved after the parylene coating.

The measured applied strain was 617.1 ± 8.5%, which corresponds to ~93% of the maximum theoretical strain from Eq. (4) (661% for $N = 2$). Location of fracture was recorded to be located at the start of the moving arm for all 3 tests. (See Supplementary Figure 1 and Video 1 showing fracture location). Fig. 3(c) and 3(d) show one of the SAS structures used for the test before fracture. Additionally, we performed a cyclic tensile test in a separate SAS sample (up to ~400% extension or ~65% from the theoretical maximum for a safety margin) using the same equipment at a moderate rate of 250 mm/min for 3000 cycles without fracture, showing remarkable endurance (see Supplementary Video 2 for a sample of the cyclic test showing 300 cycles). It is to be noted that previous demonstrations of this kind of silicon-based spiral structures have been able to demonstrate structural integrity only up to ~400 cycles [43].

On the other hand, fabricated parylene-coated SAS structures were able to reach beyond the maximum theoretical elongation. Again, 3 samples were tested, displaying an applied strain of 933 ± 43.7% or ~40% extra elongation from the theoretical maximum. The additional displacement derives from the added extension of the serpentine and horseshoe structures along the spiral's arms. Fig 3(e) shows a sample of a coated structure being completely extended before fracture. Fracture location was the same as observed in the uncoated samples. Moreover, thanks the spiral being able to reach fully extension and its improved handling, it was possible to measure the maximum load that can be held by a single structure without fracture, corresponding to ~14.7 mN. Finally, a cyclic test was also performed up to ~400% extension, but a higher cycling rate was managed, 650 mm/min, which was not attainable by the uncoated samples. The coated sample was able to endure 3000 cycles as well, maintaining its structural integrity, with no fracture being observed during or after the test. Moreover, we should point out that the higher cycling rate was achieved thanks to the better handling and stretchability displayed by

parylene-coated samples compared to uncoated ones. Thus, improved robustness is demonstrated. (see Supplementary Video 3 for a sample of the cyclic test showing 300 cycles).

4.1 Finite Element Analysis Results

Finite element analysis (FEA) was used to study the effect of defects on the stress concentration along the structure. The geometry was designed in SOLIDWORKS and then imported into COMSOL using the CAD import tool. The imported geometry in COMSOL was extruded to 50 μm and the width of the silicon arms set to be 5 μm. Silicon mechanical properties used were: Young's modulus = 165 GPa and Poisson's ratio = 0.17. The boundary conditions are set in a way that one arm is fixed while the other arm moves under a prescribed displacement. The effect of geometric non-linearity due to the large deformation of the structure was also included. Defects were included in the geometry with different sizes (0.1 μm and 1 μm) and locations along the arm (start, middle and end). A ~0.1μm defect was observed in the fabricated structures (Fig. 2(b)), while 1μm defect was added to observe the effect of bigger defects in the structure. It should be noted that defects at certain locations along the arms of the spiral are studied individually for better understanding of their independent effect.

We started our study with the straight-arm spiral without defects to use as reference. The results show that the structure reaches the silicon's ultimate tensile strength or fracture (~7 GPa [67]) when stretch to 2.125 mm displacement. Subsequently, to observe the effect of defects, we induced a small defect of 0.1 μm (comparable to the one found in fabricated structures) at the start of both arms (Fig. 4). The maximum stress was observed at the location of the defects and the displacement before fracture was reduced to 2 mm for 0.1 μm and 1.975 mm for 1 μm. This suggests that even small structural defects along the spiral's arms can cause considerable stress concentration at those sites, which then leads to

earlier structure's failure. This can provide a valid explanation why the fabricated uncoated structures were not able to reach the theoretical maximum elongation. For the case of 0.1 μm defect, the simulated structure reached failure at ~90% of the theoretical maximum displacement (from Eq. 1 and 2). More importantly, it also agrees with the observations of fracture location of practical experiments as noted earlier.

Similar results to the previous case were observed for defects at the end of the arms for both 0.1 μm and 1 μm defect sizes. However, for defects at the middle of the arms, the maximum stress was observed at the end of the arms instead of the defective site. This is due to the fact that the interfaces between the rigid island and spring-interconnects experience more stress due to external strain, as can be also appreciated in Fig. 4. Table 1 summarizes and compares the different displacements at fracture and stress values at the defect sites between straight-arm and SAS structures.

Table 1. Summary of FEA results for straight-arm as well as SAS structures, with and without defects.

Design	**Defect location along arms**	**Defect size [μm]**	**Displacement at Fracture [mm]**	**Difference in Fracture Displacement [%]**	**Stress at Defect [MPa]**
Straight-arm spiral (control structure)	**No Defect**		2.125	-	-
	Start	0.1	2	-5.88 [a]	7393*
		1	1.975	-7.06 [a]	7137*
	Middle	0.1	2.125	0.00 [a]	3175
		1	2.125	0.00 [a]	3300
	End	0.1	1.9	-10.59 [a]	7205.4*
		1	1.85	-12.94 [a]	7108.6*
SAS structure	**No Defect**		2.5	17.65 [a]	-
	Start	0.1	2.25	12.50 [b]	7088.5*
		1	2.2	11.39 [b]	7196.4*
	Middle	0.1	2.5	17.65 [b]	5375

		1	2.5	17.65 [b]	5500
	End	0.1	2.5	31.58 [b]	5195
		1	2.5	35.14 [b]	5730

[a] Comparison with respect to the value of the straight-arm spiral without defect.
[b] Comparison with respect to the corresponding defect-location and size of the straight-arm spiral.
* for these cases the structure reaches ultimate tensile strength (fracture) at the defect location. For the rest of the cases, the fracture location is at the end of the arms.

Next, the straight-arm spiral was replaced with the SAS structure. FEA results showed that the SAS structure without any defect reached silicon's ultimate tensile strength at a displacement of 2.5 mm (~17.5% longer than the straight-arm spiral). Later, defects of 0.1 μm and 1 μm were introduced at the start of the arms (Fig 5(a), 5(b)), showing that stress still localizes at these defective sites, reaching the fracture limit at a shorter displacement compared with the structure without defect, but displaying less (~40%) overall stress magnitude compared to the straight-arm design. On the other hand, defects located at the end of the arms showed a significant reduction (~80%) in the stress located at the defect compared to the straight-arm design, shifting the maximum stress localization towards the end of the arm (See Supplementary Figure 2). Finally, defects located at the middle of the arms showed a very similar behavior to the straight-arm design, with a small stress reduction of ~4% at the defect site. Table 2 shows a summary of stress reduction at defect sites between the straight-arm and SAS designs.

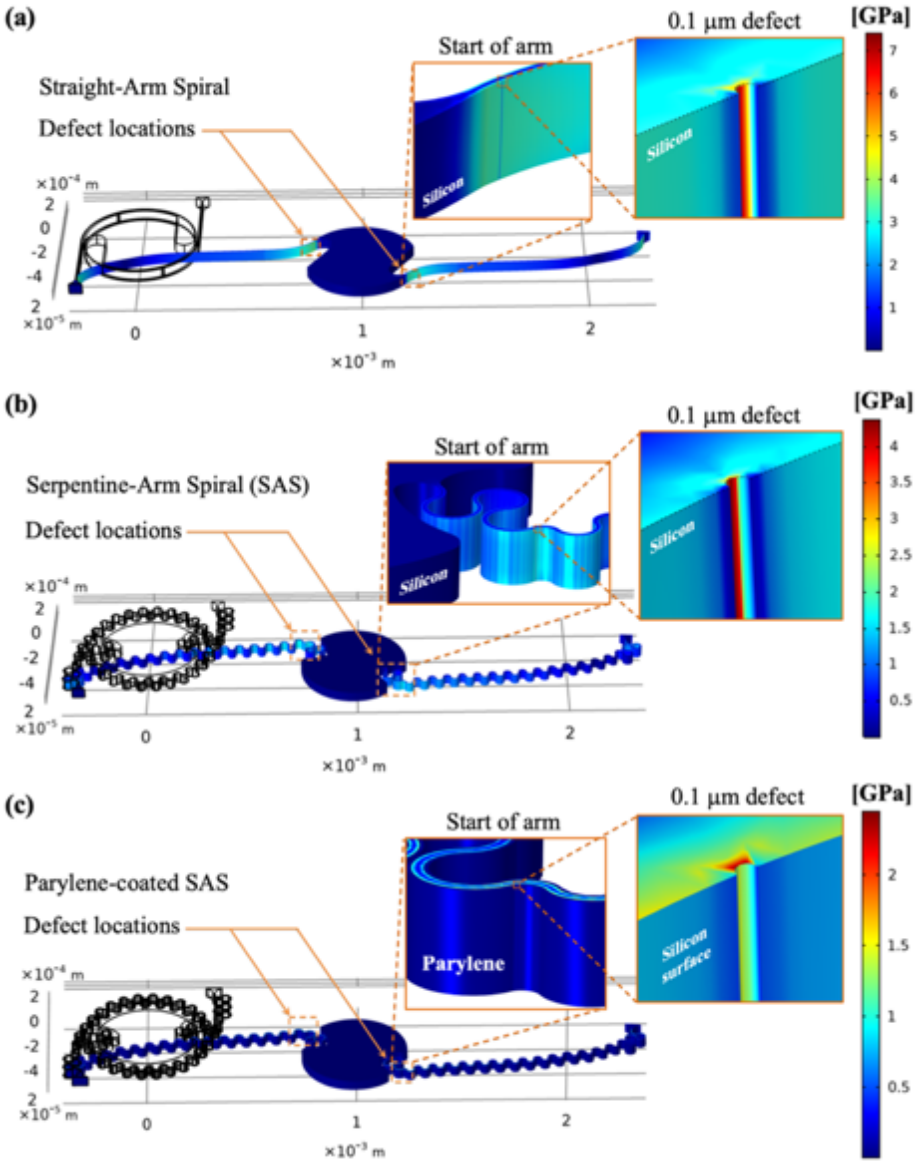

Fig. 4 Von Mises stress distribution along different designs extended up to a 2 mm displacement, with 0.1 µm defects located at the start of the arms. (a) Straight-arm spiral structure with zoom-in views at defect location. (b) SAS structure with zoom-in views at defect location. (c) SAS structure with parylene-coating and zoom-in views showing reduced stress concentration (Parylene was hidden from smaller inset to appreciate the stress at the silicon surface).

Next, FEA was used to study the effects of the polymer coating on the structures. To this purpose, a layer of polymer (Parylene type C, Young's modulus = 2.89 GPa, Poisson's ratio = 0.4, 2 µm thick), was added to the sidewalls of the silicon structure. Perfect binding was assumed between the polymer

and silicon and similar boundary conditions were used as in case of non-coated structures. Simulation results for polymer-coated, SAS structure without any defect showed no significant improvement in displacement before fracture. However, in the case of coated structures with defect at the start at the arm, above 10% longer displacement was observed. More notably, with defects at the start of the arm, there was a considerable reduction in the stress magnitude at the defective sites (Fig. 5(c)). Around 30% and 56% stress reduction were achieved for 0.1 μm and 1 μm defects respectively, between coated and uncoated structures under the same displacement. This reduction in the stress might come from the polymer filling the defective sites and helping in reducing the stress localized at the silicon surface. Defects located at the middle and end of the arms also experienced significant stress reduction compared to the uncoated structure, as can be seen in Table 2.

Table 2. Summary comparing stress at defect sites between straight-arm vs. SAS structures, and uncoated SAS vs. coated SAS structures.

Design's comparison	**Defect location along arms**	**Defect size [μm]**	**Stress Reduction [%]**
Straight-arm vs. SAS structures	Start	0.1	-38.77
		1	-33.77
	Middle	0.1	-3.81
		1	-3.22
	End	0.1	-83.28
		1	-81.89
Uncoated SAS vs. Parylene-coated SAS structures	Start	0.1	-30.03
		1	-56.87
	Middle	0.1	-23.57
		1	-30.00
	End	0.1	-16.84
		1	-25.70

A comparison between straight-arm and SAS designs, as well as the effectiveness of the parylene coating can be seen in Fig. 6 for 0.1 μm defects located at the start of the arms. It can be observed that the polymer helped in significantly reducing the stress localization of the structure under externally applied strain. (See Supplementary Figures 2 and 3 for comparison between structures with defects located at the end and middle of the arms respectively).

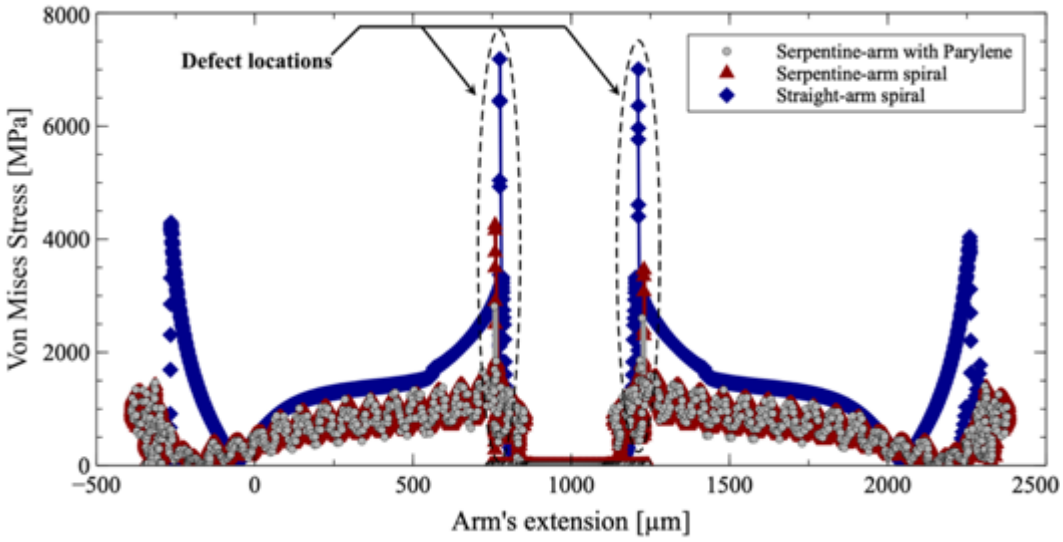

Fig. 5 Comparison at 2 mm total displacement between the stress distribution along the arms of the straight-arm spiral, un-coated SAS and parylene-coated SAS structures. (Defects are located at the start of the arms with a size of 0.1 μm).

These results show that parylene-coating is effective and helps reducing the stress localization. It is also observed that the SAS structure itself has much less stress concentration compared to straight-arm spiral. To sum up, from Table 1 and Fig. 6, it is evident that the SAS design itself shows significant improvement in stress reduction and maximum displacement before fracture. Additionally, it shows that defects located at the start of the arms are predominant for SAS structures, which is validated by the observed fracture location during practical testing. Moreover, from Table 2, the stress values at defective sites are much lower for SAS structures compared to straight-arm ones, which can be improved even further when coated with parylene. For the cases of 0.1 μm and 1 μm defects located at the start of the

arms, a remarkable ~40% and ~35% stress reduction respectively, can be achieved alone between the SAS structures and the reference straight-arm design, while coated structures achieved a ~30% and ~57% further reduction respectively. These encouraging results demonstrates the great potential of smart integration of materials and geometries to maximize mechanical robustness.

5. Conclusions

We have presented an efficient way of fabricating ultra-stretchable compound structures using standard microfabrication techniques and allowing the use of a low-cost silicon (100) substrate, which could be even recycled few times for improved cost-effectiveness. FEA showed the effectiveness of parylene coating in terms of better stress mitigation in case of defective structures with different sizes and locations. Results show that SAS structures can reach up to ~80% stress reduction at the defective location compared to straight-arm spirals, while the parylene-coating helps to reduce it up to ~60% further. Moreover, fabricated SAS structures reached up to ~600% applied strain before fracture, while parylene-coated structures were able to reach ~50% larger strain. Handling of coated samples was also improved significantly. Additionally, both SAS structures with and without coating, endured over 3000 cycles without fracture, where the parylene-coated structures were able to withstand a faster cycling rate when compared to uncoated samples.

With these results, we have provided a practical solution to lithographic defects that may happen during fabrication of spiral structures and showed a robust mechanical behavior under cyclic tensile conditions. Such development is an important advancement towards the realization of reliable, ultra-stretchable electronics for applications demanding both, high electric performance and high deformation capabilities.

Author contributions

Jhonathan P. Rojas: Conceptualization, Methodology, Supervision, Writing-Reviewing and Editing; **Mutee U. Rehman**: Investigation, Software, Data curation, Writing- Original draft preparation, **Wedyan Babatain**: Investigation; **Sohail F. Shaikh**: Investigation; **David Conchouso**: Investigation, Writing-Reviewing and Editing; **Nadeem Qaiser**: Investigation, Software. **Muhammad M. Hussain**: Resources, Writing-Reviewing and Editing.

Acknowledgment

The authors would like to acknowledge the support provided by the Deanship of Scientific Research (DSR) at King Fahd University of Petroleum & Minerals (KFUPM) for funding this work through projects No. IN161020 and No. KAUST001.

Conflicts of interest:

The authors declare no competing financial interest.

Supplementary Information

See supplementary information for figures of fracture locations and videos of cyclic tests of fabricated structures, as well as comparison of stress distribution of different designs for defects located at the middle and end of the arms.

References

[1] Y. Chen, Y.-S. Kim, B. Tillman, W.-H. Yeo, Y. Chun, Advances in Materials for Recent Low-Profile Implantable Bioelectronics, Materials (Basel). 11 (2018) 522. doi:10.3390/ma11040522.

[2] T.Q. Trung, N.E. Lee, Flexible and Stretchable Physical Sensor Integrated Platforms for Wearable Human-Activity Monitoringand Personal Healthcare, Adv. Mater. 28 (2016) 4338–4372. doi:10.1002/adma.201504244.

[3] H. Ju, J. Jeong, P. Kwak, M. Kwon, J. Lee, Robotic Flexible Electronics with Self-Bendable Films, Soft Robot. 5 (2018) 710–717. doi:10.1089/soro.2017.0141.

[4] J.A. Rogers, T. Someya, Y. Huang, Materials and Mechanics for Stretchable Electronics,

Science (80-.). 327 (2010) 1603–1607. doi:10.1126/science.1182383.
[5] C.R. Kagan, Flexible colloidal nanocrystal electronics, Chem. Soc. Rev. 48 (2019) 1626–1641. doi:10.1039/C8CS00629F.
[6] J. Prieto Rojas, M. Rehman, M. Albettar, A. Arevalo, D. Conchouso, D. Singh, I. Foulds, M.M. Hussain, Folding and stretching a thermoelectric generator, in: M.S. Islam, A.K. Dutta, T. George (Eds.), Micro- Nanotechnol. Sensors, Syst. Appl. X, SPIE, 2018: p. 13. doi:10.1117/12.2304992.
[7] B. Stadlober, M. Zirkl, M. Irimia-Vladu, Route towards sustainable smart sensors: ferroelectric polyvinylidene fluoride-based materials and their integration in flexible electronics, Chem. Soc. Rev. 48 (2019) 1787–1825. doi:10.1039/C8CS00928G.
[8] C. Wang, C. Wang, Z. Huang, S. Xu, Materials and Structures toward Soft Electronics, Adv. Mater. 30 (2018) 1801368. doi:10.1002/adma.201801368.
[9] Z. Xue, H. Song, J.A. Rogers, Y. Zhang, Y. Huang, Mechanically-Guided Structural Designs in Stretchable Inorganic Electronics, Adv. Mater. 32 (2020) 1–32. doi:10.1002/adma.201902254.
[10] Y. Wang, L. Sun, C. Wang, F. Yang, X. Ren, X. Zhang, H. Dong, W. Hu, Organic crystalline materials in flexible electronics, Chem. Soc. Rev. 48 (2019) 1492–1530. doi:10.1039/C8CS00406D.
[11] Y. Yuan, G. Giri, A.L. Ayzner, A.P. Zoombelt, S.C.B. Mannsfeld, J. Chen, D. Nordlund, M.F. Toney, J. Huang, Z. Bao, Ultra-high mobility transparent organic thin film transistors grown by an off-centre spin-coating method, Nat. Commun. 5 (2014) 1–9. doi:10.1038/ncomms4005.
[12] S. Choi, S.I. Han, D. Kim, T. Hyeon, D.-H. Kim, High-performance stretchable conductive nanocomposites: materials, processes, and device applications, Chem. Soc. Rev. 48 (2019) 1566–1595. doi:10.1039/C8CS00706C.
[13] A. Kamyshny, S. Magdassi, Conductive nanomaterials for 2D and 3D printed flexible electronics, Chem. Soc. Rev. 48 (2019) 1712–1740. doi:10.1039/C8CS00738A.
[14] S. Gao, X. Yi, J. Shang, G. Liu, R.-W. Li, Organic and hybrid resistive switching materials and devices, Chem. Soc. Rev. 48 (2019) 1531–1565. doi:10.1039/C8CS00614H.
[15] S.J. Benight, C. Wang, J.B.H. Tok, Z. Bao, Stretchable and self-healing polymers and devices for electronic skin, Prog. Polym. Sci. 38 (2013) 1961–1977. doi:10.1016/j.progpolymsci.2013.08.001.
[16] N.T. Kalyani, S.J. Dhoble, Organic light emitting diodes : Energy saving lighting technology — A review, Renew. Sustain. Energy Rev. 16 (2012) 2696–2723. doi:10.1016/j.rser.2012.02.021.
[17] J.M. Nassar, J.P. Rojas, A.M. Hussain, M.M. Hussain, From stretchable to reconfigurable inorganic electronics, Extrem. Mech. Lett. 9 (2016) 245–268. doi:10.1016/j.eml.2016.04.011.
[18] a. Nathan, A. Ahnood, M.T. Cole, Sungsik Lee, Y. Suzuki, P. Hiralal, F. Bonaccorso, T. Hasan, L. Garcia-Gancedo, A. Dyadyusha, S. Haque, P. Andrew, S. Hofmann, J. Moultrie, Daping Chu, a. J. Flewitt, a. C. Ferrari, M.J. Kelly, J. Robertson, G. a. J. Amaratunga, W.I. Milne, Flexible Electronics: The Next Ubiquitous Platform, Proc. IEEE. 100 (2012) 1486–1517. doi:10.1109/JPROC.2012.2190168.
[19] T. Someya, Y. Kato, T. Sekitani, S. Iba, Y. Noguchi, Y. Murase, H. Kawaguchi, T. Sakurai, Conformable, flexible, large-area networks of pressure and thermal sensors with organic transistor active matrixes., Proc. Natl. Acad. Sci. U. S. A. 102 (2005) 12321–12325. doi:10.1073/pnas.0502392102.
[20] T. Someya, T. Sekitani, S. Iba, Y. Kato, H. Kawaguchi, T. Sakurai, A large-area, flexible pressure sensor matrix with organic field-effect transistors for artificial skin applications., Proc. Natl. Acad. Sci. U. S. A. 101 (2004) 9966–9970. doi:10.1073/pnas.0401918101.

[21] J.P. Rojas, A. Arevalo, I.G. Foulds, M.M. Hussain, Design and characterization of ultra-stretchable monolithic silicon fabric, Appl. Phys. Lett. 105 (2014) 154101. doi:10.1063/1.4898128.
[22] W.S. Wong, A. Salleo, Flexible Electronics: Materials and Applications, 2009. doi:10.1007/978-0-387-74363-9.
[23] J.A. Rogers, R. Ghaffari, D.-H. Kim, Stretchable Bioelectronics for Medical Devices and Systems, Springer International Publishing, Cham, 2016. doi:10.1007/978-3-319-28694-5.
[24] G.A. Torres Sevilla, N. Qaiser, M.D. Cordero, S.F. Shaikh, M.M. Hussain, Fully spherical stretchable silicon photodiodes array for simultaneous 360 imaging, Appl. Phys. Lett. 113 (2018) 134101. doi:10.1063/1.5049233.
[25] M.U. Rehman, J.P. Rojas, Optimization of compound serpentine–spiral structure for ultra-stretchable electronics, Extrem. Mech. Lett. 15 (2017) 44–50. doi:10.1016/j.eml.2017.05.004.
[26] N. Qaiser, S.M. Khan, M. Nour, M.U. Rehman, J.P. Rojas, M.M. Hussain, Mechanical response of spiral interconnect arrays for highly stretchable electronics, Appl. Phys. Lett. 111 (2017) 214102. doi:10.1063/1.5007111.
[27] J.A. Rogers, Materials for semiconductor devices that can bend, fold, twist, and stretch, Mrs Bull. 39 (2014) 549–556. doi:10.1557/mrs.2014.102.
[28] S. Il Park, J.H. Ahn, X. Feng, S. Wang, Y. Huang, J.A. Rogers, Theoretical and experimental studies of bending of inorganic electronic materials on plastic substrates, Adv. Funct. Mater. 18 (2008) 2673–2684. doi:10.1002/adfm.200800306.
[29] P. Mandlik, S.P. Lacour, J.W. Li, S.Y. Chou, S. Wagner, Fully elastic interconnects on nanopatterned elastomeric substrates, IEEE Electron Device Lett. 27 (2006) 650–652. doi:10.1109/LED.2006.879029.
[30] S.P. Lacour, C. Tsay, S. Wagner, An elastically stretchable TFT Circuit, IEEE Electron Device Lett. 25 (2004) 792–794. doi:10.1109/LED.2004.839227.
[31] D.S. Gray, J. Tien, C.S. Chen, High-Conductivity Elastomeric Electronics (Adv. Mater. 2004, 16, 393.), Adv. Mater. 16 (2004) 477–477. doi:10.1002/adma.200490017.
[32] H. Fu, S. Xu, R. Xu, J. Jiang, Y. Zhang, J.A. Rogers, Y. Huang, Lateral buckling and mechanical stretchability of fractal interconnects partially bonded onto an elastomeric substrate, Appl. Phys. Lett. 106 (2015) 91902. doi:10.1063/1.4913848.
[33] Y. Su, Z. Liu, S. Kim, J. Wu, Y. Huang, J.A. Rogers, Mechanics of stretchable electronics with high fill factors, Int. J. Solids Struct. 49 (2012) 3416–3421. doi:10.1016/j.ijsolstr.2012.07.024.
[34] D.H. Kim, Z. Liu, Y.S. Kim, J. Wu, J. Song, H.S. Kim, Y. Huang, K.C. Hwang, Y. Zhang, J.A. Rogers, Optimized structural designs for stretchable silicon integrated circuits, Small. 5 (2009) 2841–2847. doi:10.1002/smll.200900853.
[35] K.D. Harris, A.L. Elias, H.J. Chung, Flexible electronics under strain: a review of mechanical characterization and durability enhancement strategies, J. Mater. Sci. 51 (2016) 2771–2805. doi:10.1007/s10853-015-9643-3.
[36] D.-H. Kim, N. Lu, Y. Huang, J. a. Rogers, Materials for stretchable electronics in bioinspired and biointegrated devices, MRS Bull. 37 (2012) 226–235. doi:10.1557/mrs.2012.36.
[37] D.-H. Kim, J. Song, W.M. Choi, H.-S. Kim, R.-H. Kim, Z. Liu, Y.Y. Huang, K.-C. Hwang, Y. Zhang, J.A. Rogers, Materials and noncoplanar mesh designs for integrated circuits with linear elastic responses to extreme mechanical deformations., Proc. Natl. Acad. Sci. U. S. A. 105 (2008) 18675–18680. doi:10.1073/pnas.0807476105.
[38] J. a Fan, W.-H. Yeo, Y. Su, Y. Hattori, W. Lee, S.-Y. Jung, Y. Zhang, Z. Liu, H. Cheng, L. Falgout, M. Bajema, T. Coleman, D. Gregoire, R.J. Larsen, Y. Huang, J. a Rogers, Fractal

design concepts for stretchable electronics., Nat. Commun. 5 (2014) 3266. doi:10.1038/ncomms4266.
[39] Z. Yan, F. Zhang, F. Liu, M. Han, D. Ou, Y. Liu, Q. Lin, X. Guo, H. Fu, Z. Xie, M. Gao, Y. Huang, J. Kim, Y. Qiu, K. Nan, J. Kim, P. Gutruf, H. Luo, A. Zhao, K.-C. Hwang, Y. Huang, Y. Zhang, J.A. Rogers, Mechanical assembly of complex, 3D mesostructures from releasable multilayers of advanced materials, Sci. Adv. 2 (2016) e1601014. doi:10.1126/sciadv.1601014.
[40] S. Xu, Y. Zhang, J. Cho, J. Lee, X. Huang, L. Jia, J.A. Fan, Y. Su, J. Su, H. Zhang, H. Cheng, B. Lu, C. Yu, C. Chuang, T. Kim, T. Song, K. Shigeta, S. Kang, C. Dagdeviren, I. Petrov, P. V. Braun, Y. Huang, U. Paik, J.A. Rogers, Stretchable batteries with self-similar serpentine interconnects and integrated wireless recharging systems, Nat. Commun. 4 (2013) 1543. doi:10.1038/ncomms2553.
[41] C. Lv, H. Yu, H. Jiang, Archimedean spiral design for extremely stretchable interconnects, Extrem. Mech. Lett. 1 (2014) 29–34. doi:10.1016/j.eml.2014.12.008.
[42] K. Huang, R. Dinyari, G. Lanzara, Y.K. Jong, J. Feng, C. Vancura, F.K. Chang, P. Peumans, An approach to cost-effective, robust, large-area electronics using monolithic silicon, Tech. Dig. - Int. Electron Devices Meet. IEDM. (2007) 217–220. doi:10.1109/IEDM.2007.4418906.
[43] N. Qaiser, A.N. Damdam, S.M. Khan, S.F. Shaikh, M.M. Hussain, Design , mechanics , and operation of spiral- interconnect based networked sensor for stretchable electronics, 115 (2019). doi:10.1063/1.5123680.
[44] N. Qaiser, A.N. Damdam, S.M. Khan, S.F. Shaikh, M.M. Hussain, Mirror-symmetry controlled mechanical response of interconnects for stretchable electronics, Extrem. Mech. Lett. 35 (2020) 100639. doi:10.1016/j.eml.2020.100639.
[45] R.W. Odom, J.A. Chakel, D.F. Reich, SURFACE ANALYSIS OF INORGANIC AND ORGANIC PARTICLES ON SILICON, in: Dennis N. Schmidt (Ed.), Proc. Symp. Contam. Control Defect Reduct. Semicond. Manuf. III, The Electrochemical Society, Inc., 1994: pp. 40–46.
[46] C.R. Brundle, Y.S. Uritsky, Full Wafer Particle Defect Characterization, 285 (2001). doi:10.1063/1.1354412.
[47] T.A. Desai, D. Hansford, M. Ferrari, Characterization of micromachined silicon membranes for immunoisolation and bioseparation applications, J. Memb. Sci. 159 (1999) 221–231. doi:10.1016/S0376-7388(99)00062-9.
[48] S.K. Tewksbury, Wafer-Level Integrated Systems, Springer US, Boston, MA, 1989. doi:10.1007/978-1-4613-1625-1.
[49] J. Prieto Rojas, Organic-inorganic heterostructures for stretchable electronics, in: M.S. Islam, T. George (Eds.), Micro- Nanotechnol. Sensors, Syst. Appl. XI, SPIE, 2019: p. 40. doi:10.1117/12.2519017.
[50] J.P. Rojas, G.A. Torres Sevilla, M.T. Ghoneim, S. Bin Inayat, S.M. Ahmed, A.M. Hussain, M.M. Hussain, Transformational Silicon Electronics, ACS Nano. 8 (2014) 1468–1474. doi:10.1021/nn405475k.
[51] G.T. Sevilla, J.P. Rojas, S. Ahmed, A. Hussain, S. Bin Inayat, M.M. Hussain, SILICON FABRIC FOR MULTI-FUNCTIONAL APPLICATIONS Integrated Nanotechnology Lab , King Abdullah University of Science and Technology , Saudi Arabia, (2013) 2636–2639.
[52] E.A. Baisie, M. Yang, R. Kaware, M. Hooker, Z.C. Li, W. Sun, X.H. Zhang, An economic study on chemical mechanical polishing of silicon wafers, in: Proc. ASME Int. Manuf. Sci. Eng. Conf. 2009, MSEC2009, American Society of Mechanical Engineers Digital Collection, 2009: pp. 691–696. doi:10.1115/MSEC2009-84072.

[53] A. Krueger, M. Lisker, A. Trusch, A. Mai, CMP Process for Wafer Backside Planarization, ICPT 2017; Int. Conf. Planarization/CMP Technol. Proc. (2017) 1–5.
[54] R. Martini, H. Sivaramakrishnan Radhakrishnan, V. Depauw, K. Van Nieuwenhuysen, I. Gordon, M. Gonzalez, J. Poortmans, Improvement of seed layer smoothness for epitaxial growth on porous silicon, in: Mater. Res. Soc. Symp. Proc., Cambridge University Press, 2013: pp. 97–102. doi:10.1557/opl.2013.748.
[55] M. Yang, M. Ieong, L. Shi, K. Chan, V. Chan, A. Chou, E. Gusev, K. Jenkins, D. Boyd, Y. Ninomiya, D. Pendleton, Y. Surpris, D. Heenan, J. Ott, K. Guarini, C. D'Emic, M. Cobb, P. Mooney, B. To, N. Rovedo, J. Benedict, R. Mo, H. Ng, High Performance CMOS Fabricated on Hybrid Substrate with Different Crystal Orientations, Tech. Dig. - Int. Electron Devices Meet. (2003) 453–456. doi:10.1109/iedm.2003.1269320.
[56] J.P. Rojas, A. Syed, M.M. Hussain, Mechanically Flexible Optically Transparent Porous Mono-Crystalline Silicon Substrate, in: Micro Electro Mech. Syst., IEEE, Paris, France, 2012: pp. 281–284.
[57] J.P. Rojas, G. a Torres Sevilla, M.M. Hussain, Can we build a truly high performance computer which is flexible and transparent?, Sci. Rep. 3 (2013) 2609. doi:10.1038/srep02609.
[58] Y.-H. Kim, E. Lee, J.G. Um, M. Mativenga, J. Jang, Highly Robust Neutral Plane Oxide TFTs Withstanding 0.25 mm Bending Radius for Stretchable Electronics, Sci. Rep. 6 (2016) 25734. doi:10.1038/srep25734.
[59] L. Mao, Q. Meng, A. Ahmad, Z. Wei, Mechanical analyses and structural design requirements for flexible energy storage devices, Adv. Energy Mater. 7 (2017) 1–19. doi:10.1002/aenm.201700535.
[60] X. Dong, M. Zhang, Y. Lei, Z. Li, Y. Jin, W. Wang, Parylene-MEMS technique-based flexible electronics, Sci. China Inf. Sci. 61 (2018) 60419. doi:10.1007/s11432-018-9430-2.
[61] S. Kuppusami, R.H. Oskouei, Parylene Coatings in Medical Devices and Implants: A Review, Univers. J. Biomed. Eng. 3 (2015) 9–14. doi:10.13189/ujbe.2015.030201.
[62] M. Golda-Cepa, K. Engvall, M. Hakkarainen, A. Kotarba, Recent progress on parylene C polymer for biomedical applications: A review, Prog. Org. Coatings. 140 (2020) 105493. doi:10.1016/j.porgcoat.2019.105493.
[63] Y. Li, Q. Xie, W. Wang, M. Zheng, H. Zhang, Y. Lei, H.A. Zhang, W. Wu, Z. Li, Parylene C-on-photoresist (POP): A low temperature spacer scheme for polymer/metal nanowire fabrication, J. Micromechanics Microengineering. 21 (2011) 67001. doi:10.1088/0960-1317/21/6/067001.
[64] Y. Chen, W. Pei, R. Tang, S. Chen, H. Chen, Conformal coating of parylene for surface anti-adhesion in polydimethylsiloxane (PDMS) double casting technique, Sensors Actuators, A Phys. 189 (2013) 143–150. doi:10.1016/j.sna.2012.09.024.
[65] F. Rizzi, A. Qualtieri, L.D. Chambers, W.M. Megill, M. De Vittorio, Parylene conformal coating encapsulation as a method for advanced tuning of mechanical properties of an artificial hair cell, Soft Matter. 9 (2013) 2584–2588. doi:10.1039/c2sm27566j.
[66] H.I. Kuo, R. Zhang, W.H. Ko, Development of micropackage technology for biomedical implantable microdevices using parylene C as water vapor barrier coatings, in: Proc. IEEE Sensors, 2010: pp. 438–441. doi:10.1109/ICSENS.2010.5690184.
[67] K.E. Petersen, Silicon as a mechanical material, Proc. IEEE. 70 (1982) 420–457. doi:10.1109/PROC.1982.12331.